Supplement of Atmos. Chem. Phys., 24, 10475–10512, 2024
https://doi.org/10.5194/acp-24-10475-2024-supplement

Supplement of

Measurement report: Source attribution and estimation of black carbon levels in an urban hotspot of the central Po Valley – an integrated approach combining high-resolution dispersion modelling and micro-aethalometers

Giorgio Veratti et al.

Correspondence to: Giorgio Veratti (giorgio.veratti@unimore.it)

Table S1. Comparison of MAE values used in this study with measurements from different European sites. The values in brackets represent the minimum and maximum MAE values observed during the reference period, while the mean MAE plus or minus the standard deviation is indicated.

Reference	Location	Type of sampling site	Instrument for b_{abs}	Period	Wavelength (nm)	MAE ($m^2\ g^{-1}$)
This study	-	-	-	-	880	10.120
					625	14.091
					528	17.070
					470	19.070
					375	24.069
Savadkoohi et al. (2024)	Athens (GR)	urban background	AE33	2017-2020	880	6.1 ± 4.0
	Marseille (FR)	urban background	AE33	2014-2019	880	5.1 ± 1.7
	Zurich (CH)	urban background	AE33	2012-2021	880	4.9 ± 2.3
	Rome (IT)	urban background	AE33	2019-2022	880	8.8 ± 3.1
	Elche (SP)	urban background	AE33	2022-2023	880	7.3 ± 2.1
	Athens (GR)	suburban	AE33	2017-2019	880	10.1 ± 2.3
	Bern (CH)	urban traffic	AE31-AE33	2015-2021	880	5.7 ± 3.5
	Paris (FR)	suburban	AE31-AE33	2012-2021	880	5.5 ± 3.0
	Payerne (CH)	rural background	AE31-AE33	2012-2021	880	12.4 ± 4.1
	London (UK)	urban background	AE22	2009-2019	880	8.8 ± 2.6
	London (UK)	urban traffic	AE22	2009-2019	880	9.7 ± 1.8
	Helsinki (FN)	urban traffic	MAAP	2015-2019	637	12.4 ± 4.7
	Leipzig (DE)	urban traffic	MAAP	2011-2019	637	13.8 ± 4.6
	Dresden (DE)	urban traffic	MAAP	2017-2019	637	9.6 ± 2.6
	Barcelona (SP)	urban background	MAAP	2009-2021	637	9.6 ± 2.6
	Granada (SP)	urban background	MAAP	2006-2020	637	10.4 ± 3.3
	Dresden (DE)	urban background	MAAP	2017-2019	637	10.4 ± 4.1
	Milan (IT)	urban background	MAAP	2013-2021	637	11.2 ± 6.5
	Prague (CZ)	urban background	MAAP	2021-2022	637	14.0 ± 3.7
	Hyytiälä (FN)	rural background	MAAP	2013-2021	637	7.3 ± 4.7
	Ispra (IT)	rural background	MAAP	2008-2020	637	10.8 ± 4.4
Mbengue et al. (2021)	Kramolín (CZ)	rural background	AE31	2017	950	4.14 ± 1.39
					880	4.93 ± 1.96
					660	6.71 ± 2.28
					590	7.35 ± 2.57
					520	8.46 ± 3.00
					470	10.34 ± 3.71
					370	12.16 ± 4.72
Yuan et al. (2021)	Melpitz (DE)	regional background	PAX	Feb 2017	870	7.4 (7.2-7.9)
Ciupek et al. (2021)	London (UK)	urban traffic	AE22	2019	880	7.8 (6.0-9.8)
		urban background		2018		7.8 (6.0-9.8)
Gilardoni et al. (2020)	Milan (IT)	urban background	AE22	Feb 2016	880	9.8 ± 2.2
	Motta Visconti (IT)	rural background		Feb-Mar 2016		10.5 ± 1.1
Grange et al. (2020)	Switzerland	4 rural and 2 urban sites	AE33	2008-2018	950	11.3 ± 2.9 [a]
Mousavi et al. (2019)	Milan (IT)	urban background	AE31	2017-2018	880	9.5 ± 1.3
					370	16.5 ± 0.6
	Bareggio (IT)	rural background	AE51	2017-2018	880	8.5 ± 1.2
					370	16.2 ± 1.2
Zanatta et al. (2016)	Aspvreten (SE)	regional background	PSAP	2010-2011	637	8.38 ± 1.22
	Birkenes (NO)	regional background	PSAP	2010-2011	637	8.09 ± 1.33
	Finokalia (GR)	rural background	PSAP	2008-2010	637	15.1 ± 1.75
	Puy de Dôme (FR)	rural background	PSAP	2010-2011	637	7.04 ± 1.87
	Harwell (UK)	regional background	MAAP	2010	637	8.87 ± 1.84
	Ispra (IT)	rural background	MAAP	2008-2011	637	9.31 ± 1.35
	Melpitz (DE)	regional background	MAAP	2008-2010	637	8.22 ± 1.47
	Montseny (SP)	rural background	MAAP	2008-2011	637	8.29 ± 1.82
Laborde et al. (2013)	Paris (FR)	suburban	AE31	Jan-Feb 2010	880	8.6 (7.3-8.8)

[a] Average value of six different sites, four of rural background (Payerne, Magadino-Cadenazzo, San Vittore and Rigi-Seebodenalp), one of urban background (Zurich-Kaserne) and one of urban traffic (Bern-Bollwerk).

S1 Analysis of the absorption Ångström exponent

Combustion sources such as wood burning and traffic emissions have distinct wavelength-dependent light absorption signatures, particularly in the ultraviolet and lower visible range. This characteristic fingerprint allows their contribution to be identified from the total measured absorption Zotter et al. (2017); Sandradewi et al. (2008); Massabò et al. (2015); Bernardoni et al. (2017). The absorption Ångström exponent (α) serves as a single parameter to quantify the source-specific dependence of light absorption coefficient on wavelength. In the absence of validation measurements, the α frequency distribution can guide the estimation of suitable α values for the source apportionment model. Figure S1 shows the probability density function of α for the hourly aggregated measurements during the two periods analysed in the main text, i.e. from 4 February to 7 March 2020 and from 26 December 2020 to 21 January 2021 at the traffic site, and from 4 February to 7 March 2020 and from 26 December 2020 to 7 January 2021 at the background site. Data reported with light blue colour are calculated as follow:

$$\alpha = -\frac{\log(b_{880}/b_{375})}{\log(880/375)}$$

Where b_{880} and b_{375} are the absorption coefficients at 880 nm and 375 nm respectively. While the data shown in grey are obtained by fitting the absorption coefficient as a function of the five wavelengths (375, 470, 528, 625 and 880 nm) with a filter of $r^2 > 0.99$ to the fit. In addition, a subplot for the traffic site has been incorporated under its facet, showing α values only for the morning rush hour (08:00 GMT time) on working days, i.e. when the traffic contribution is expected to be at its peak. For traffic, the source-specific α value is set to 1, which corresponds to the centre of the probability density function (PDF) distribution for the morning rush hour on working days at the traffic site. Conversely, the α value for biomass burning is set to 2, representing the upper tail of the stringent-filtered PDF distribution for both traffic and background sites, as suggested by Tobler et al. (2021).

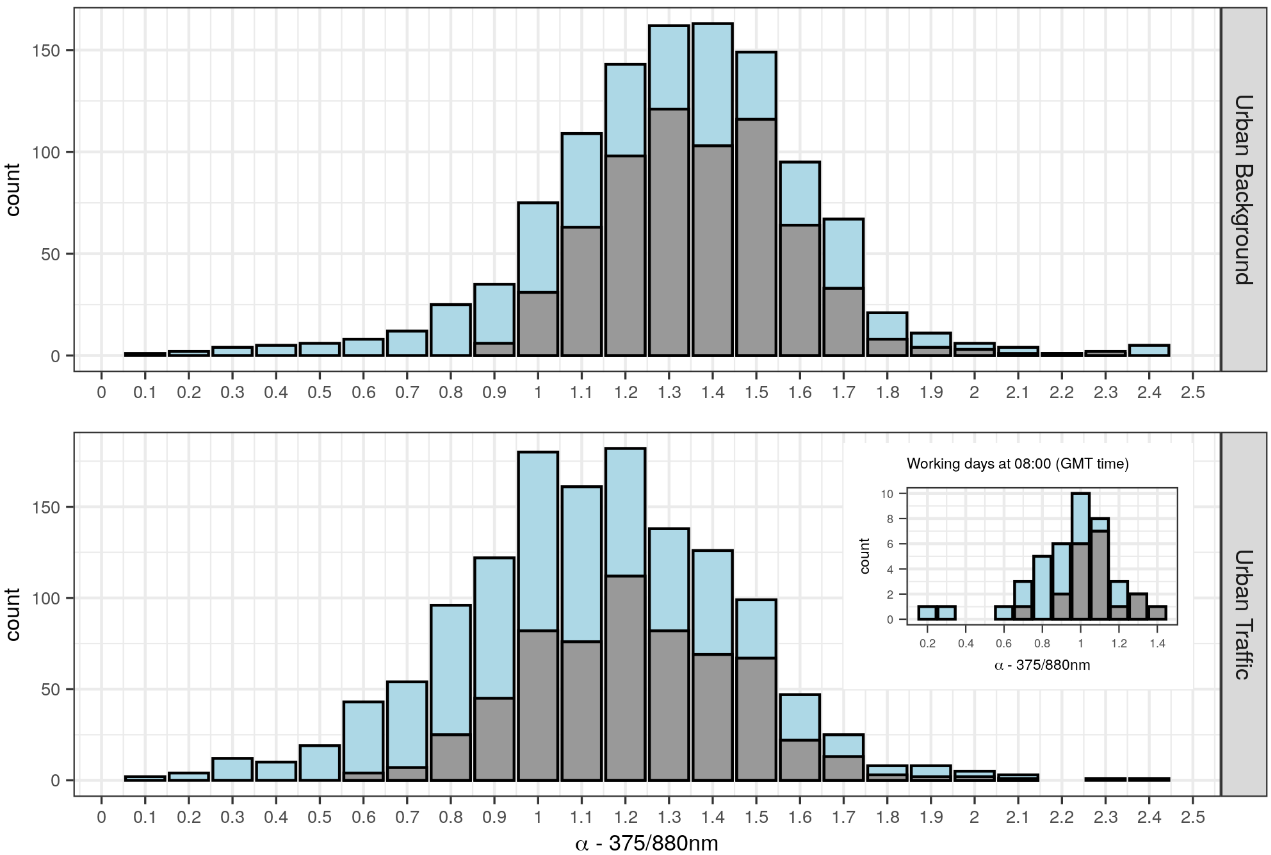

Figure S1. The absorption Ångström exponent (α) probability density function calculated from the ratio of the 375 nm and 880 nm wavelengths and from the fit off all wavelengths from 375 nm to 880 nm and filtered for fit $r^2 > 0.99$.

S2 BC speciation factors

Table S2. BC speciation factors from $\mathrm{PM}_{2.5}$ emissions and BC emission factors (EF) expressed as g of BC per GJ or kWh net thermal input (with related 95% confidence intervals).

Emission Sector	Emission activity	Fuel	BC/$\mathrm{PM}_{2.5}$ (%)	BC EF
Energy production	all	liquid	56	1.081 (0.05–5.04) g Gj^{-1}
Energy production	all	biomass and agricultural residues	6.4	4.389 (2.178–8.778) g Gj^{-1}
Energy production	all	CNG	4	0.0056 g Gj^{-1}
Domestic heating	open fireplaces	biomass	7	57.4 (28.7–114.8) g Gj^{-1}
Domestic heating	conventional stoves burning	biomass	10	74 (37–148) g Gj^{-1}
Domestic heating	high-efficiency stoves	biomass	16	59.2 (45.6–118.4) g Gj^{-1}
Domestic heating	advanced/ecolabelled stoves and boilers	biomass	28	44.8 (22.4–89.6) g Gj^{-1}
Domestic heating	pellet stoves and boilers	biomass	15	9 (4.5–18) g Gj^{-1}
Domestic heating	all	CNG	5.4	0.119 (0.07–0.167) g Gj^{-1}
Industry	all	solid fuel	6.4	6.912 (3.84–14.08) g Gj^{-1}
Industry	all	CNG	4	0.0312 (0.019–0.014) g Gj^{-1}
Industry	all	liquid	56	11.2 (6.72–15.68) g Gj^{-1}
Other mobile machinery	all	liquid	70	0.78 (1.540–0.002) g kWh^{-1}
Waste management	incinerator	all	20	0.105 (0.038–0.29) g Gj^{-1}

S3 Model evaluation

To evaluate the performance of the models in reproducing BC concentrations and wind speed, several statistical indicators were considered. These indicators were derived by considering M as the modelled values, O as the observations, n as the count of model-observation pairs,

$$\bar{M} = \frac{1}{n}\sum_{i=1}^{n} M_i$$

as the average modelled value, and

$$\bar{O} = \frac{1}{n}\sum_{i=1}^{n} O_i$$

as the average observed value. The following metrics were employed for evaluation:

$$MB = \frac{1}{n}\sum_{i=1}^{n}(M_i - O_i)$$

$$NMB = \frac{1}{n}\sum_{i=1}^{n}\frac{(M_i - O_i)}{O_i}$$

$$r = \frac{\sum_{i=1}^{n}(M_i - \bar{M})(O_i - \bar{O})}{\sqrt{\sum_{i=1}^{n}(M_i - \bar{M})^2 \sum_{i=1}^{n}(O_i - \bar{O})^2}}$$

$$FAC2 = \text{Fraction of data where } 0.5 \leq \frac{M_i}{O_i} \leq 2$$

$$NMSE = \frac{\overline{(O - M)^2}}{\bar{O} \cdot \bar{M}}$$

$$FB = \frac{\overline{O - M}}{0.5 \cdot (\bar{O} + \bar{M})}$$

$$NAD = \frac{\overline{|O - M|}}{(\bar{O} + \bar{M})}$$

$$RMSE = \sqrt{\frac{1}{n}\sum_{i=1}^{n}(M_i - O_i)^2}$$

S4 Meteorological analysis

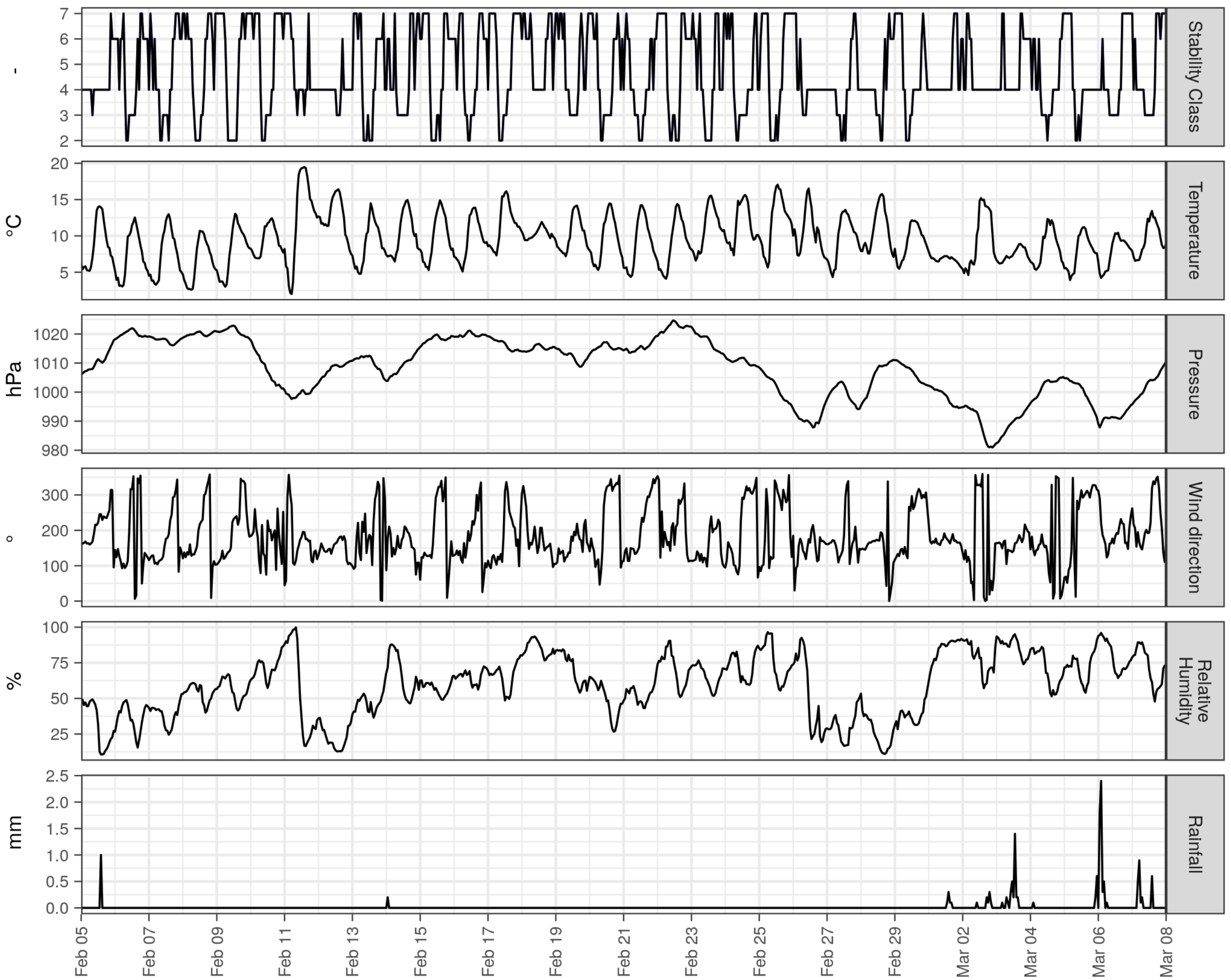

Figure S2. Hourly time series of measured (temperature, pressure, wind direction, relative humidity, rainfall) and estimated (stability class) meteorological parameters during the first period (4 February - 7 March 2020) at OSS station.

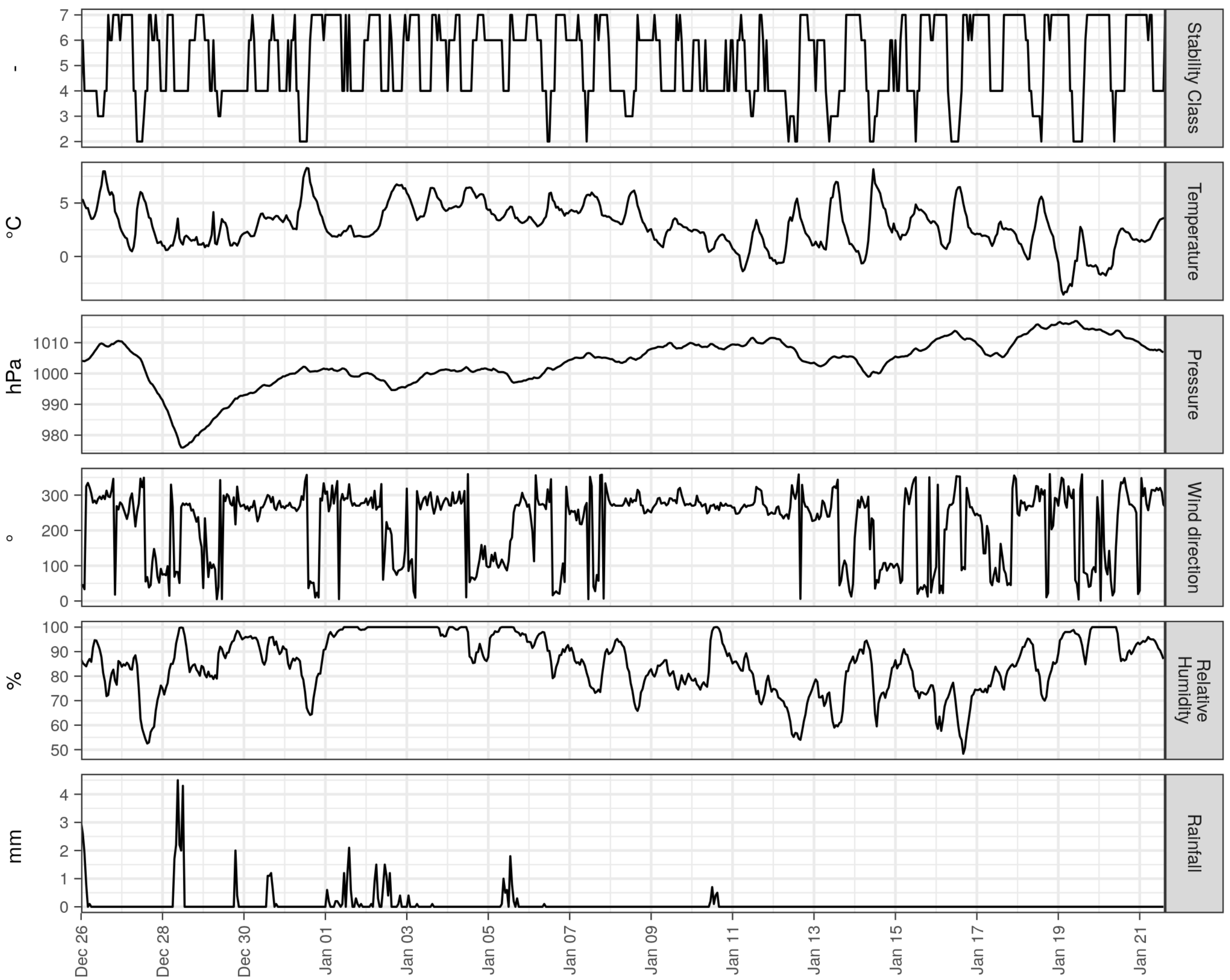

Figure S3. Hourly time series of measured (temperature, pressure, wind direction, relative humidity, rainfall) and estimated (stability class) meteorological parameters during the second period (26 December 2020 - 21 January 2021) at OSS station.

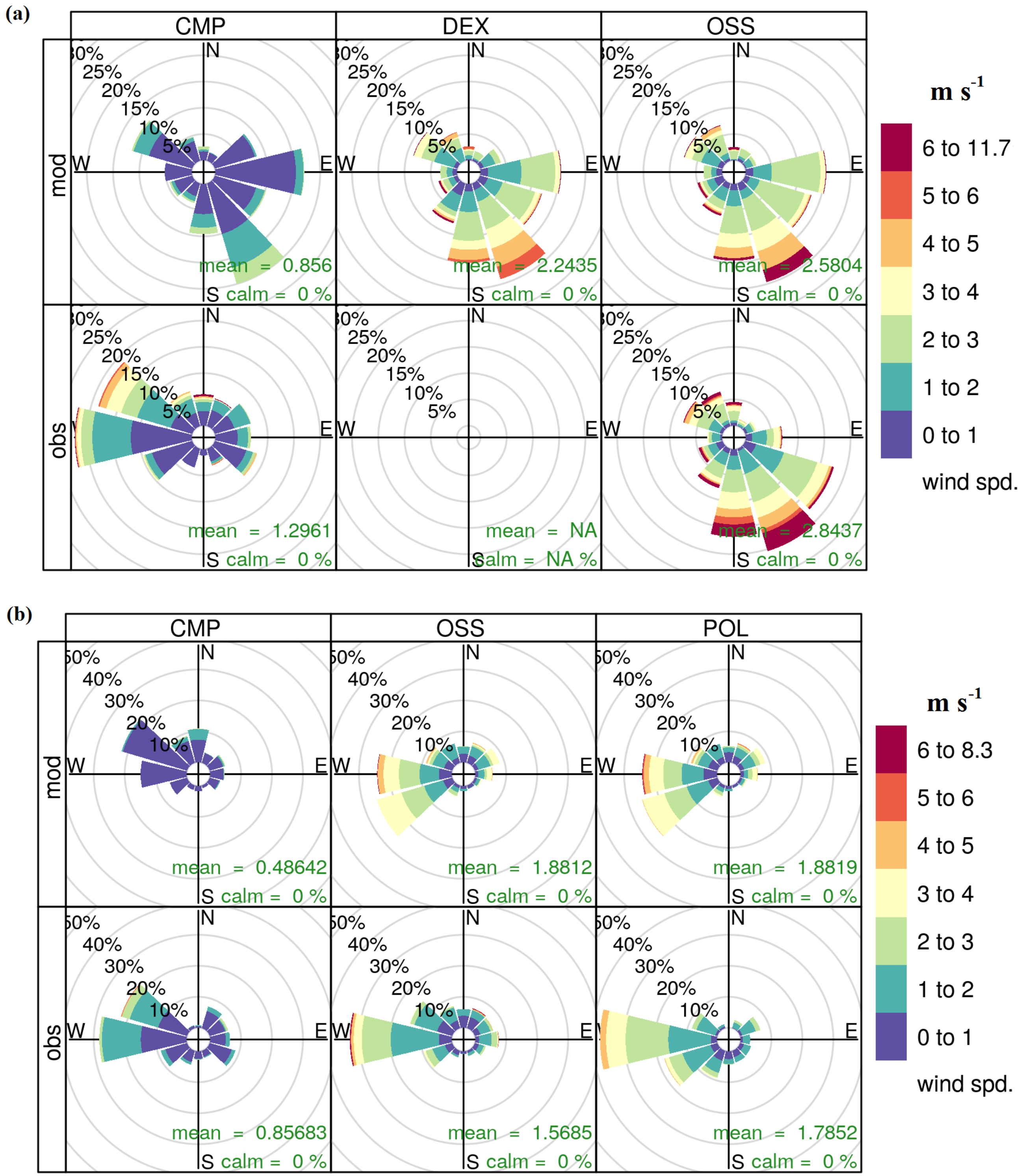

Figure S4. Comparison of modelled (mod) and observed (obs) wind roses at CMP, OSS, DEX and POL stations for the two simulation periods: (a) first period (4 February - 7 March 2020) and (b) second period (26 December 2020 - 21 January 2021). Wind direction data from DEX station during the first period were excluded from the analysis due to a significant data gap and observed biases in the sensor readings.

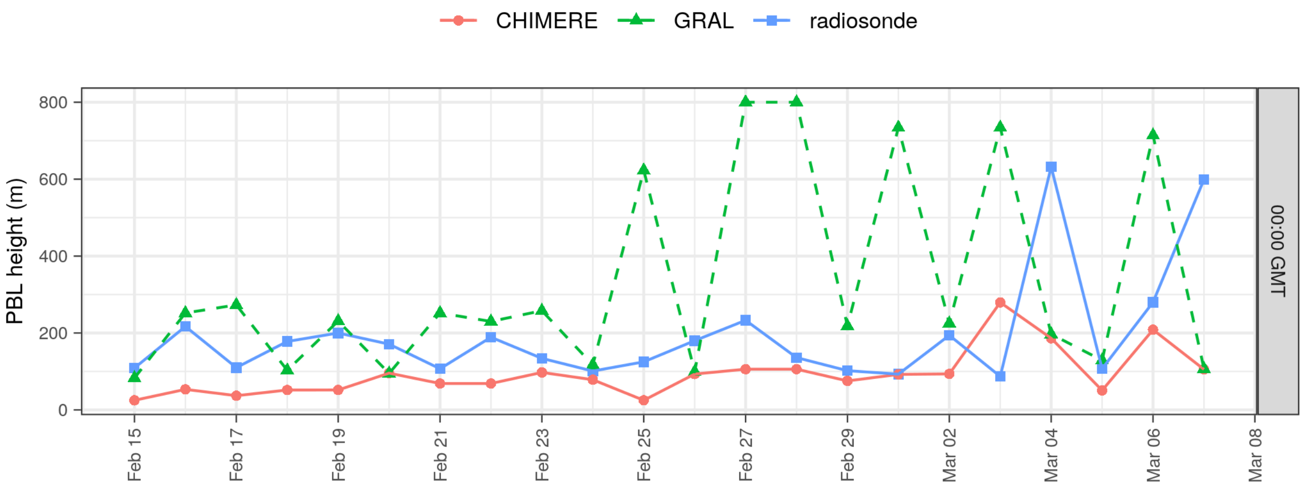

Figure S5. Comparison of the estimated PBL height from soundings (blue) and CHIMERE simulations (orange) at the SPC station for the first simulated period (4 February - 7 March 2020) at 00:00 GMT. For qualitative comparison, the PBL height simulated by GRAL over the urban area of Modena is also included (green).

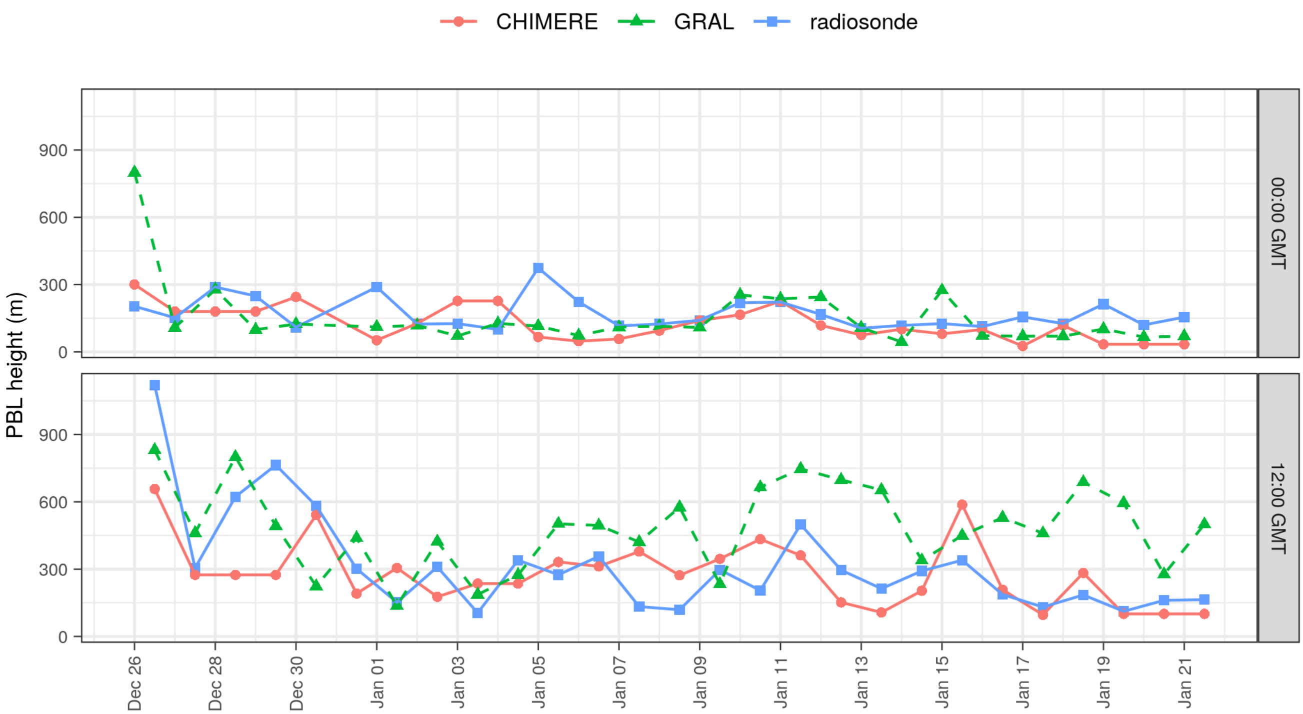

Figure S6. Comparison of the estimated PBL height from soundings (blue) and CHIMERE simulations (orange) at the SPC station for the second simulated period (26 December 2020 - 21 January 2021) at 00:00 and 12:00 GMT. For qualitative comparison, the PBL height simulated by GRAL over the urban area of Modena is also included (green).

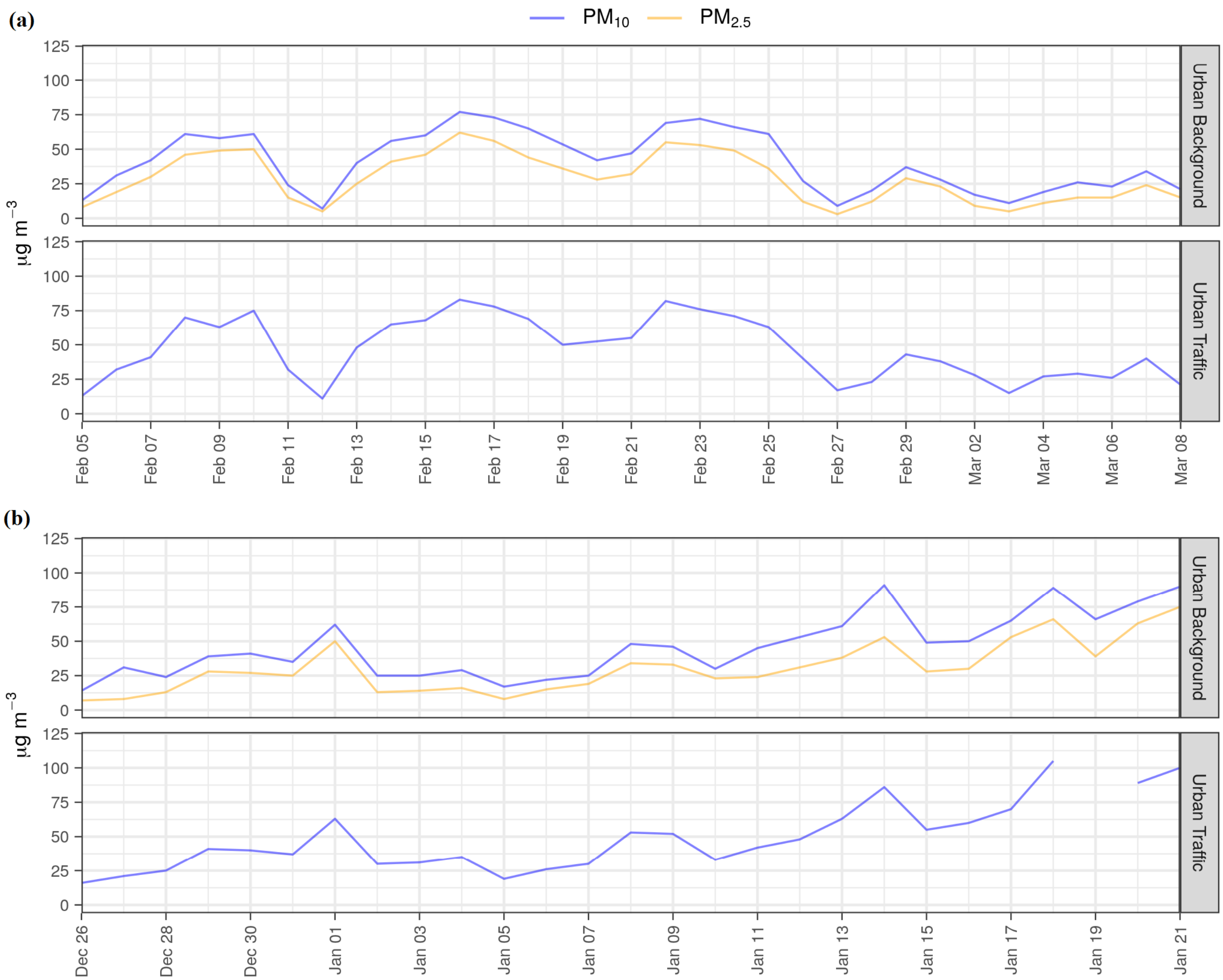

Figure S7. Daily time series of measured PM_{10} and $\mathrm{PM}_{2.5}$ concentrations at urban traffic and background sites for the first period, panel (a), and the second period, panel (b).

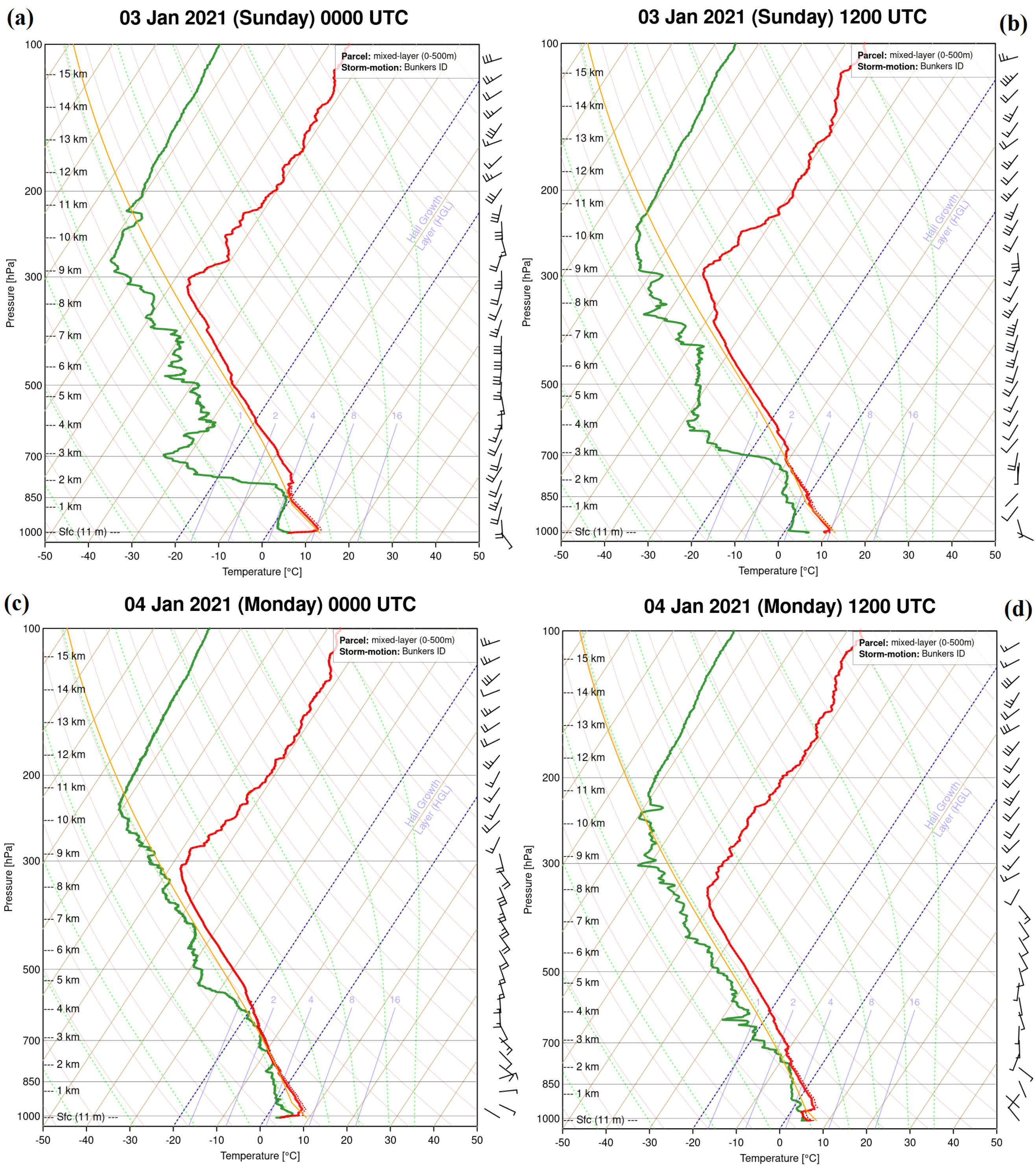

Figure S8. Skew-T Log-P plot from S. Pietro Capofiume station on 3 January 2021 on the first row (panels a and b) and on 4 January 2021 on the second row (panels c and d), at 00:00 GMT on the left, and at 12:00 GMT on the right. The red line represents the temperature of the atmosphere, while the green line represents the dewpoint.

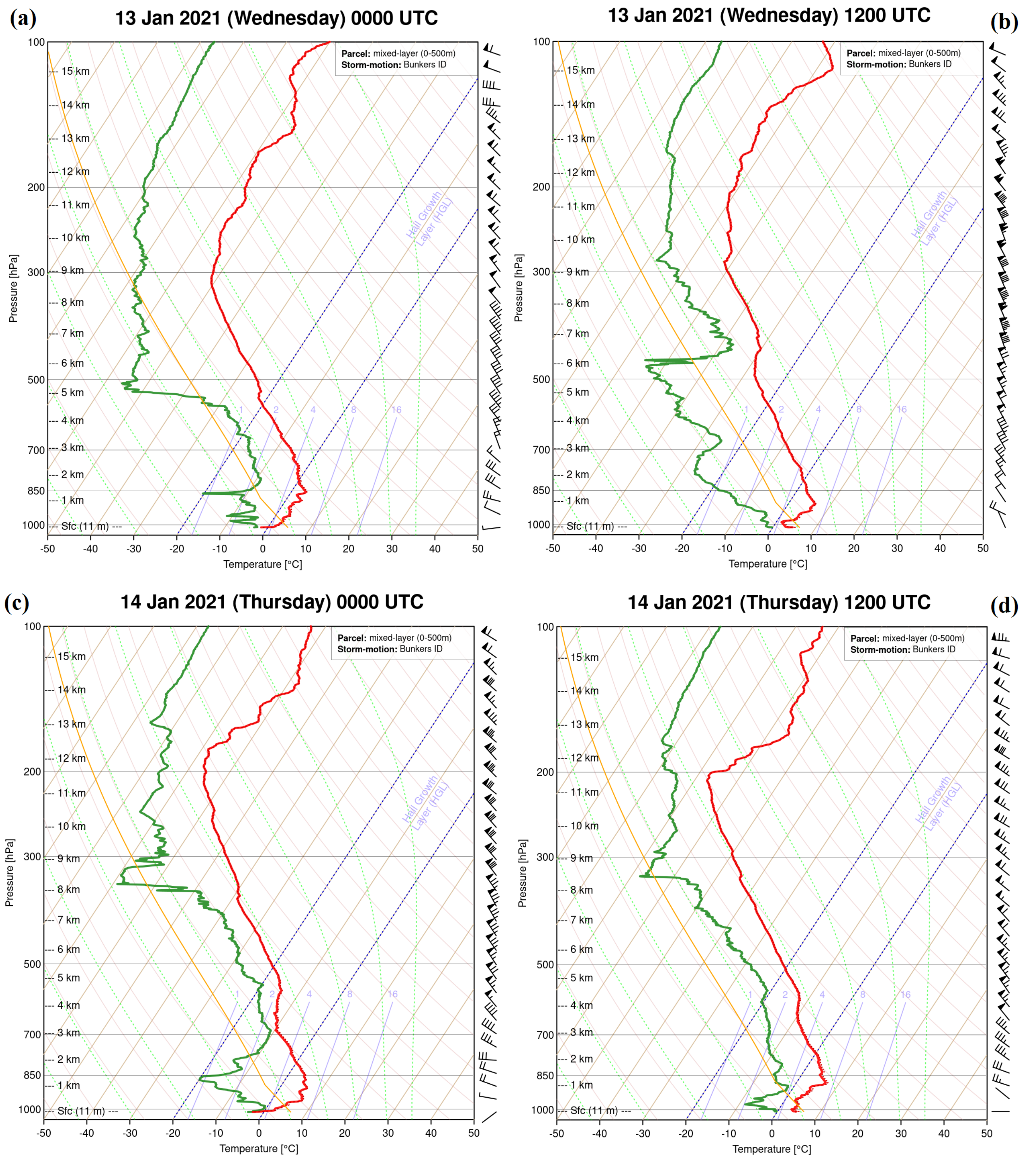

Figure S9. Skew-T Log-P plot from S. Pietro Capofiume station on 13 January 2021 on the first row (panels a and b) and on 14 January 2021 on the second row (panels c and d), at 00:00 GMT on the left, and at 12:00 GMT on the right. The red line represents the temperature of the atmosphere, while the green line represents the dewpoint.

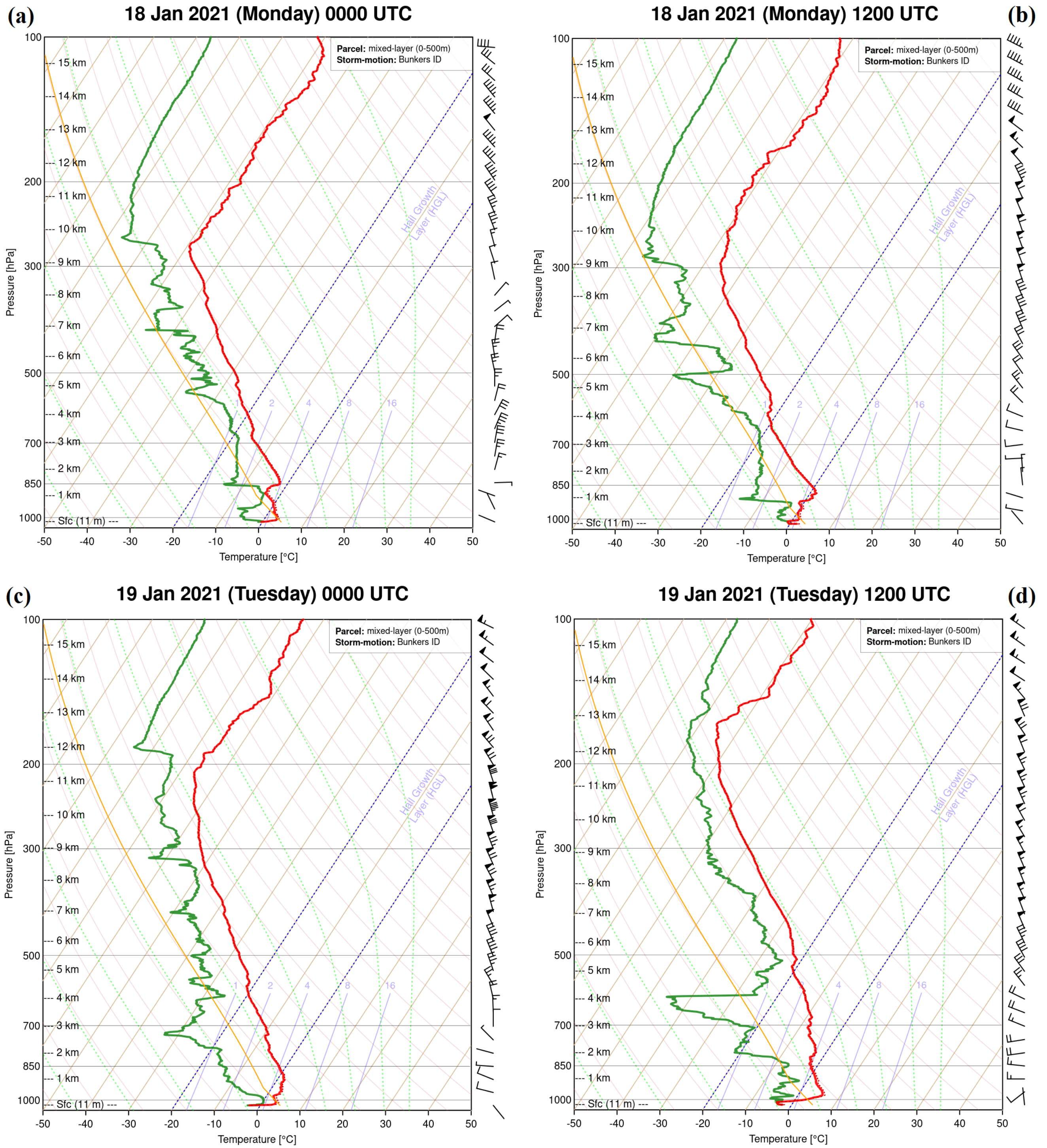

Figure S10. Skew-T Log-P plot from S. Pietro Capofiume station on 18 January 2021 on the first row (panels a and b) and on 19 January 2021 on the second row (panels c and d), at 00:00 GMT on the left, and at 12:00 GMT on the right. The red line represents the temperature of the atmosphere, while the green line represents the dewpoint.

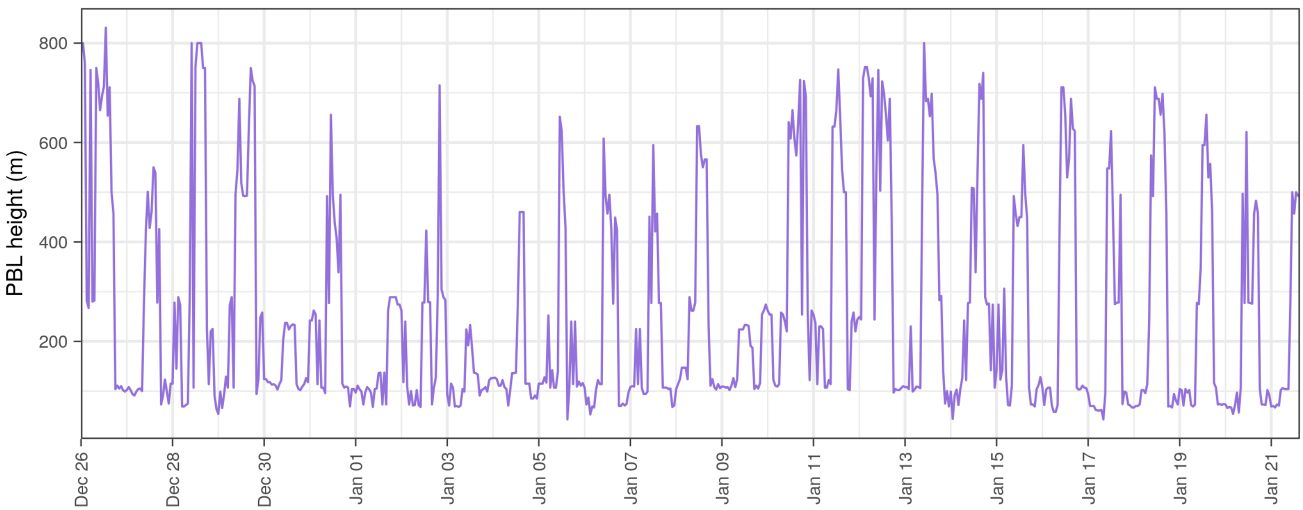

Figure S11. Hourly time series of modelled Planetary Boundary Layer height by GRAL over the urban area of Modena for the second period.

S5 Daily emission modulations

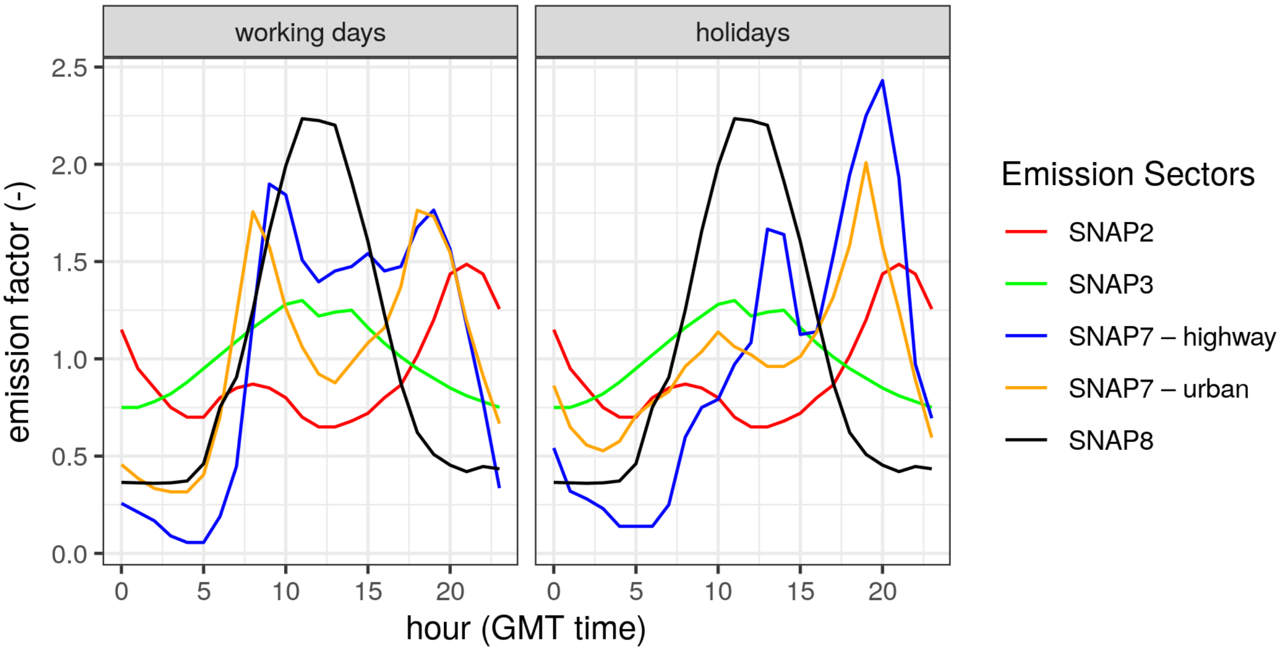

Figure S12. Daily modulation profile of BC emission sources on working days (on the left) and holidays (on the right).

S6 Linear regression analysis between modelled and measured BC concentrations

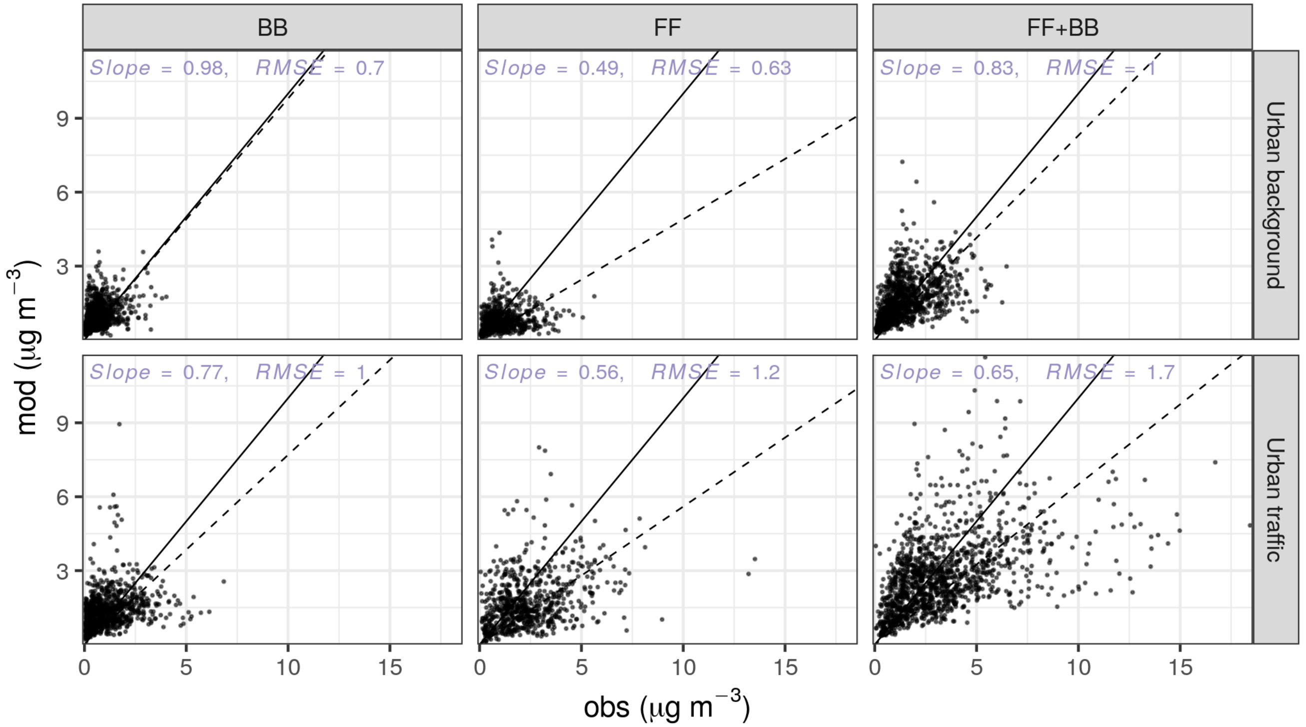

Figure S13. Linear regression between modelled and measured BC concentrations for Biomass Burning-derived BC (left panels), Fossil Fuel-derived BC (central panels) and total BC concentrations (right panels). Data include concentrations for both time periods simulated in this study.

Table S3. Results of the linear regression (slope and RMSE) for the three scenarios analysed and statistical scores (MB, NMB and FAC2) from the comparison between modelled and measured BC concentrations.

MAE at 880 nm ($m^2\,g^{-1}$)	site	source	slope	RMSE ($\mu g\,m^{-3}$)	MB ($\mu g\,m^{-3}$)	NMB (%)	FAC2 (%)
10.12	Urban traffic	FF+BB	0.65	1.72	-0.52	-16	72
	Urban traffic	FF	0.56	1.22	-0.68	-28	59
	Urban traffic	BB	0.77	1.03	0.24	22	51
	Urban background	FF+BB	0.83	1.00	0.11	7	68
	Urban background	FF	0.49	0.63	-0.32	-28	58
	Urban background	BB	0.98	0.70	0.31	43	53
8.096	Urban traffic	FF+BB	0.81	2.15	0.18	5	72
	Urban traffic	FF	0.70	1.52	-0.24	-10	61
	Urban traffic	BB	0.96	1.28	0.58	53	46
	Urban background	FF+BB	1.03	1.26	0.52	34	62
	Urban background	FF	0.61	0.78	-0.12	-10	61
	Urban background	BB	1.23	0.88	0.57	78	45
12.144	Urban traffic	FF+BB	0.54	1.44	-0.98	-30	67
	Urban traffic	FF	0.47	1.01	-0.96	-40	51
	Urban traffic	BB	0.64	0.86	0.02	2	53
	Urban background	FF+BB	0.69	0.84	-0.16	-11	71
	Urban background	FF	0.41	0.52	-0.45	-40	55
	Urban background	BB	0.82	0.58	0.14	19	59

S7 Fleet composition and BC traffic emission factors

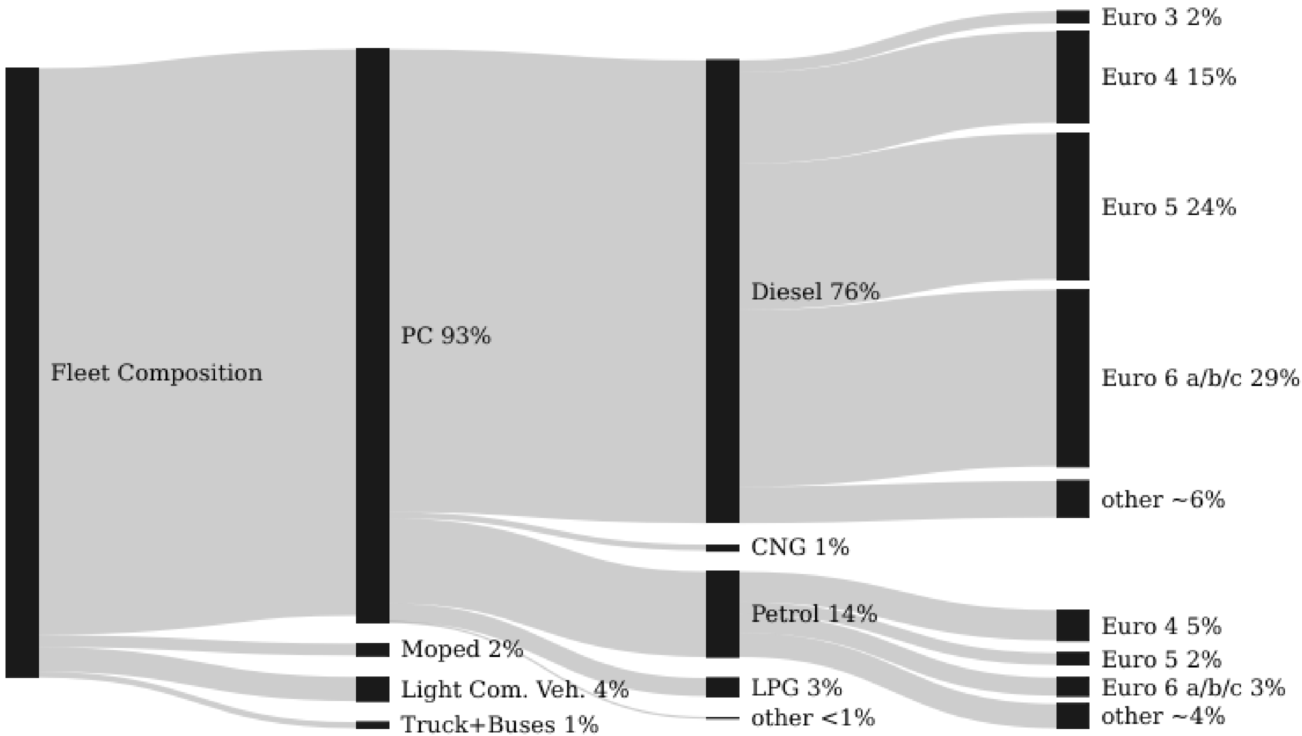

Figure S14. Local Fleet Composition. The number of registered vehicles is normalised taking into account the estimated total kilometres travelled by each vehicle category per year.

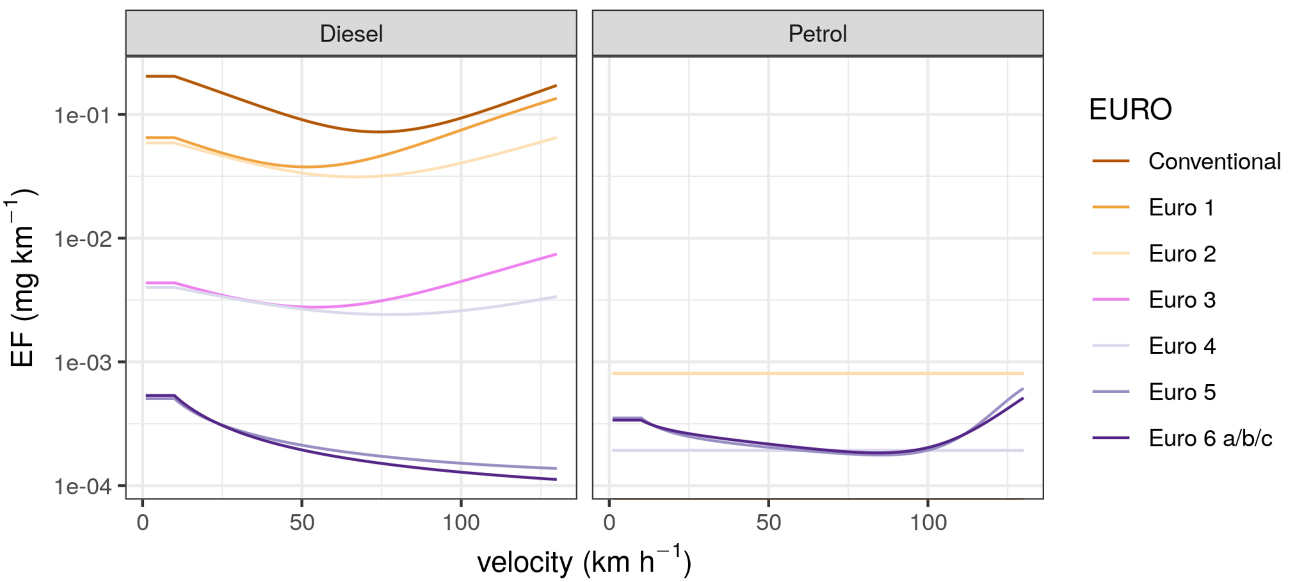

Figure S15. BC emission factors (EF) of diesel and petrol passenger cars as a function of travelling speed, as implemented in the VERT R package used in this study to estimate exhaust vehicle emissions. EF function for Petrol Conventional and Euro 1 overlaps with that of Euro 2. The same is for the curves of Petrol Euro 3 and Euro 4.

References

Bernardoni, V., Pileci, R. E., Caponi, L., and Massabò, D.: The Multi-Wavelength Absorption Analyzer (MWAA) Model as a Tool for Source and Component Apportionment Based on Aerosol Absorption Properties: Application to Samples Collected in Different Environments, Atmosphere, 8, 218, https://doi.org/10.3390/atmos8110218, number: 11 Publisher: Multidisciplinary Digital Publishing Institute, 2017.

Ciupek, K., Quincey, P., Green, D. C., Butterfield, D., and Fuller, G. W.: Challenges and policy implications of long-term changes in mass absorption cross-section derived from equivalent black carbon and elemental carbon measurements in London and south-east England in 2014–2019, Environmental Science: Processes & Impacts, 23, 1949–1960, https://doi.org/10.1039/D1EM00200G, publisher: The Royal Society of Chemistry, 2021.

Ghermandi, G., Fabbi, S., Bigi, A., Veratti, G., Despini, F., Teggi, S., Barbieri, C., and Torreggiani, L.: Impact assessment of vehicular exhaust emissions by microscale simulation using automatic traffic flow measurements, Atmospheric Pollution Research, 10, 1473–1481, https://doi.org/10.1016/j.apr.2019.04.004, 2019.

Laborde, M., Crippa, M., Tritscher, T., Jurányi, Z., Decarlo, P. F., Temime-Roussel, B., Marchand, N., Eckhardt, S., Stohl, A., Baltensperger, U., Prévôt, A. S. H., Weingartner, E., and Gysel, M.: Black carbon physical properties and mixing state in the European megacity Paris, Atmospheric Chemistry and Physics, 13, 5831–5856, https://doi.org/10.5194/acp-13-5831-2013, publisher: Copernicus GmbH, 2013.

Massabò, D., Caponi, L., Bernardoni, V., Bove, M. C., Brotto, P., Calzolai, G., Cassola, F., Chiari, M., Fedi, M. E., Fermo, P., Giannoni, M., Lucarelli, F., Nava, S., Piazzalunga, A., Valli, G., Vecchi, R., and Prati, P.: Multi-wavelength optical determination of black and brown carbon in atmospheric aerosols, Atmospheric Environment, 108, 1–12, https://doi.org/10.1016/j.atmosenv.2015.02.058, 2015.

Mbengue, S., Zikova, N., Schwarz, J., Vodička, P., Šmejkalová, A. H., and Holoubek, I.: Mass absorption cross-section and absorption enhancement from long term black and elemental carbon measurements: A rural background station in Central Europe, Science of The Total Environment, 794, 148 365, https://doi.org/10.1016/j.scitotenv.2021.148365, 2021.

Nordmann, S., Birmili, W., Weinhold, K., Müller, K., Spindler, G., and Wiedensohler, A.: Measurements of the mass absorption cross section of atmospheric soot particles using Raman spectroscopy, Journal of Geophysical Research: Atmospheres, 118, 12,075–12,085, https://doi.org/10.1002/2013JD020021, _eprint: https://onlinelibrary.wiley.com/doi/pdf/10.1002/2013JD020021, 2013.

Pandolfi, M., Ripoll, A., Querol, X., and Alastuey, A.: Climatology of aerosol optical properties and black carbon mass absorption cross section at a remote high-altitude site in the western Mediterranean Basin, Atmospheric Chemistry and Physics, 14, 6443–6460, https://doi.org/10.5194/acp-14-6443-2014, publisher: Copernicus GmbH, 2014.

Sandradewi, J., Prévôt, A. S. H., Szidat, S., Perron, N., Alfarra, M. R., Lanz, V. A., Weingartner, E., and Baltensperger, U.: Using Aerosol Light Absorption Measurements for the Quantitative Determination of Wood Burning and Traffic Emission Contributions to Particulate Matter, Environmental Science & Technology, 42, 3316–3323, https://doi.org/10.1021/es702253m, publisher: American Chemical Society, 2008.

Grange, S. K., Lötscher, H., Fischer, A., Emmenegger, L., and Hueglin, C.: Evaluation of equivalent black carbon source apportionment using observations from Switzerland between 2008 and 2018, Atmospheric Measurement Techniques, 13, 1867–1885, https://doi.org/10.5194/amt-13-1867-2020, publisher: Copernicus GmbH, 2020.

Savadkoohi, M., Pandolfi, M., Favez, O., Putaud, J.-P., Eleftheriadis, K., Fiebig, M., Hopke, P. K., Laj, P., Wiedensohler, A., Alados-Arboledas, L., Bastian, S., Chazeau, B., María, C., Colombi, C., Costabile, F., Green, D. C., Hueglin, C., Liakakou, E., Luoma, K., Listrani, S., Mihalopoulos, N., Marchand, N., Močnik, G., Niemi, J. V., Ondráček, J., Petit, J.-E., Rattigan, O. V., Reche, C., Timonen, H., Titos, G., Tremper, A. H., Vratolis, S., Vodička, P., Funes, E. Y., Zíková, N., Harrison, R. M., Petäjä, T., Alastuey, A., and Querol, X.: Recommendations for reporting equivalent black carbon (eBC) mass concentrations based on long-term pan-European in-situ observations, Environment International, 185, 108 553, https://doi.org/10.1016/j.envint.2024.108553, 2024.

Tobler, A. K., Skiba, A., Canonaco, F., Močnik, G., Rai, P., Chen, G., Bartyzel, J., Zimnoch, M., Styszko, K., Nęcki, J., Furger, M., Różański, K., Baltensperger, U., Slowik, J. G., and Prevot, A. S. H.: Characterization of non-refractory (NR) PM_1 and source apportionment of organic aerosol in Kraków, Poland, Atmospheric Chemistry and Physics, 21, 14 893–14 906, https://doi.org/10.5194/acp-21-14893-2021, publisher: Copernicus GmbH, 2021.

Yuan, J., Modini, R. L., Zanatta, M., Herber, A. B., Müller, T., Wehner, B., Poulain, L., Tuch, T., Baltensperger, U., and Gysel-Beer, M.: Variability in the mass absorption cross section of black carbon (BC) aerosols is driven by BC internal mixing state at a central European background site (Melpitz, Germany) in winter, Atmospheric Chemistry and Physics, 21, 635–655, https://doi.org/10.5194/acp-21-635-2021, publisher: Copernicus GmbH, 2021.

Zanatta, M., Gysel, M., Bukowiecki, N., Müller, T., Weingartner, E., Areskoug, H., Fiebig, M., Yttri, K. E., Mihalopoulos, N., Kouvarakis, G., Beddows, D., Harrison, R. M., Cavalli, F., Putaud, J. P., Spindler, G., Wiedensohler, A., Alastuey, A., Pandolfi, M., Sellegri, K., Swietlicki, E., Jaffrezo, J. L., Baltensperger, U., and Laj, P.: A European aerosol phenomenology-5: Climatology of black carbon optical properties at 9 regional background sites across Europe, Atmospheric Environment, 145, 346–364, https://doi.org/10.1016/j.atmosenv.2016.09.035, 2016.

Zotter, P., Herich, H., Gysel, M., El-Haddad, I., Zhang, Y., Močnik, G., Hüglin, C., Baltensperger, U., Szidat, S., and Prévôt, A. S. H.: Evaluation of the absorption Ångström exponents for traffic and wood burning in the Aethalometer-based source apportionment using radiocarbon measurements of ambient aerosol, Atmospheric Chemistry and Physics, 17, 4229–4249, https://doi.org/10.5194/acp-17-4229-2017, publisher: Copernicus GmbH, 2017.

Gilardoni, S., Massoli, P., Marinoni, A., Mazzoleni, C., Freedman, A., Lonati, G., Iuliis, S. D., and Gianelle, V.: Spatial and Temporal Variability of Carbonaceous Aerosol Absorption in the Po Valley, Aerosol and Air Quality Research, 20, 2624–2639, https://doi.org/10.4209/aaqr.2020.03.0085, publisher: Taiwan Association for Aerosol Research, 2020.

Mousavi, A., Sowlat, M. H., Lovett, C., Rauber, M., Szidat, S., Boffi, R., Borgini, A., De Marco, C., Ruprecht, A. A., and Sioutas, C.: Source apportionment of black carbon (BC) from fossil fuel and biomass burning in metropolitan Milan, Italy, Atmospheric Environment, 203, 252–261, https://doi.org/10.1016/j.atmosenv.2019.02.009, 2019.